Journal of Optics

PAPER

Polarization-enabled tunable focusing by visible-light metalenses with geometric and propagation phase

To cite this article: Jianlei Zhang *et al* 2019 *J. Opt.* **21** 115102

View the article online for updates and enhancements.

IOP ebooks™

Bringing you innovative digital publishing with leading voices to create your essential collection of books in STEM research.

Start exploring the collection - download the first chapter of every title for free.

This content was downloaded from IP address 218.22.21.24 on 21/10/2019 at 03:26

IOP Publishing Journal of Optics
J. Opt. 21 (2019) 115102 (6pp) https://doi.org/10.1088/2040-8986/ab48cf

Polarization-enabled tunable focusing by visible-light metalenses with geometric and propagation phase

Jianlei Zhang[1], Lei Zhang[2,4], Kun Huang[3], Zuoliang Duan[1] and Feng Zhao[1]

[1] School of Electronic Engineering, Xi'an University of Posts & Telecommunications, Xi'an 710121, People's Republic of China
[2] Key Laboratory for Physical Electronics and Devices of the Ministry of Education and Shaanxi Key Lab of Information Photonic Technique, School of Electronic Science and Engineering, Xi'an Jiaotong University, Xi'an 710049, People's Republic of China
[3] Department of Optics and Optical Engineering, University of Science and Technology of China, Hefei 230026, People's Republic of China

E-mail: eiezhanglei@xjtu.edu.cn

Received 17 July 2019, revised 2 September 2019
Accepted for publication 27 September 2019
Published 16 October 2019

Abstract

Flat metalenses with tunable focal length have wide applications in modern optical systems with high integration requirement. Here, by combining propagation phase and geometric phase, we numerically realize a metalens with a tunable focal length by controlling the polarization state of incident light. The tuning range can be as large as 15λ at the designer wavelength. Furthermore, the tunable performance can operate at the entire visible band with an efficiency over 35%. We believe that the proposed polarization-enabled tunable focusing metalens will find significant applications in imaging and sensing applications.

Supplementary material for this article is available online

Keywords: metalens, tunable focusing, polarization state, geometric phase

(Some figures may appear in colour only in the online journal)

1. Introduction

Optical lenses have been widely applied to imaging and display devices. Conventional refractive lenses obtain the required phase delay during light propagation. However, due to the limited refractive index, the volume of these lenses is usually bulky and thus hard to meet the miniaturization requirement in modern optical devices. In contrast, it is found that an arbitrary phase delay can also be provided by sub-wavelength structures based on various mechanisms, such as electromagnetic resonance and geometric phase [1, 2]. The related area, termed as a metasurface with planar features, has attracted increasing attention due to its flexible design scheme and great reduction in fabrication burden [3, 4]. In particular, by elaborately manipulation the phase delay distribution, metasurfaces can act as a metalens with a single focus or multifocal function [5–11]. In contrast to the continuous phase distribution used in conventional lenses, the phase delay of a metalens is discretized into several phase steps ranging from 0 to 2π and arranged according to the wavefront engineering requirement. Furthermore, with these sub-wavelength structures, metalenses can be readily integrated into miniaturized optical devices, such as spectroscopy and augment reality devices [12, 13].

Due to the extensive flexibility of phase generator, metalenses could support more interesting focusing effect [14]. However, the focal length of refractive lenses usually is fixed for given materials and curvature radius. Lately, substantial attention has been drawn to metasurfaces with tunable and reconfigurable functionalities, such as graphene metasurface

[4] Author to whom any correspondence should be addressed.

 © 2019 IOP Publishing Ltd Printed in the UK

with the tunability of reflection angles [15], tunable wave plate using phase change material [16], beam shaping based on coding metasurface [17] and switching of infrared light [18]. Especially, to tune the focal length, various efforts have been explored either by changing the immediate environment via thermo-optic effect [19, 20] and liquid crystals [21] or by altering the construction units via applied voltage [22, 23]. Besides, the phase gradient can also be reformed by stretching the elastic substrate using mechanical strain or by utilizing micro-electro-mechanical systems (MEMSs) [24–27]. However, the tuning performances such as precision and refresh rate are usually restrained by the material response. In comparison, all-optical focusing of light can be tuned much faster via coherent absorption in a plasmonic metasurface [28]. Nevertheless, current reconfigurable or dynamic methods are still challenging to realize tunable focusing of visible light at sub-wavelength level.

Alternatively, polarization states of electromagnetic wave can be used to switch the electromagnetic resonance and its associated phase/amplitude [29, 30]. By employing polarization-dependent phase control elements, polarization-switchable metasurfaces, such as hologram, light splitting, and spin-orbital interaction, have been widely investigated [31–33].

Here, we propose a polarization-enabled tuning of focal length by combining geometric and propagation phases. By judiciously selecting the phase elements, the focal length of metalens can be tuned from 88.9 to 98.6 μm at the designer wavelength with a focusing efficiency over 59%. Furthermore, the broadband tunable performance can operate at the entire visible band with a considerable efficiency. We believe that the proposed polarization-dependent focusing metalens will find significant applications in imaging and sensing applications and the design mechanism can be extended to other metasurface-based applications.

2. Principle of the proposed method

Geometric phase can only pass an equivalent phase delay with an opposite sign to right-circularly polarized (RCP) light and left-circularly polarized (LCP) light [34–36]. As a result, when two circularly polarized lights (CPLs) with opposite helicities are incident on a geometric phase based metalens, they will be focused or defocused with the same focal length [5]. Therefore, the propagation behavior of both CPLs can only be manipulate in a conjugated way using geometric phase. On the other hand, propagation phase based on resonant modes can induce a polarization-dependent phase using anisotropic structures, which can facilitate two-fold functionalities with one metasurface. However, such mechanism can only work when the incident light is linearly polarized. To manipulate two orthogonal CPLs independently, one feasible approach could be imposing arbitrary and independent phase profiles by combining the geometric and propagation phases [31, 32].

As schematically shown in figure 1, a metalens with tunable focal length is proposed by rotating the polarization state of a linearly polarized light. Initially, we can set the focal length of a metalens for RCP and LCP light to be f_1 and f_2, respectively. When the incident light is a plane wave, the required phase profiles for the RCP and LCP incident light can be respectively expressed as

$$\begin{cases} \varphi_1^{\mathrm{RCP}}(x, y) = -\dfrac{2\pi}{\lambda}(f_1 - \sqrt{x^2 + y^2 + f_1^2}) \\ \varphi_2^{\mathrm{LCP}}(x, y) = -\dfrac{2\pi}{\lambda}(f_2 - \sqrt{x^2 + y^2 + f_2^2}) \end{cases}, \tag{1}$$

where λ is the operation wavelength. Note that equation (1) can be rewritten as

$$\begin{cases} \varphi_1^{\mathrm{RCP}}(x, y) = -\dfrac{\pi}{\lambda}[(f_1 - \sqrt{x^2 + y^2 + f_1^2}) + (f_2 - \sqrt{x^2 + y^2 + f_2^2})] \\ \qquad\qquad - \dfrac{\pi}{\lambda}[(f_1 - \sqrt{x^2 + y^2 + f_1^2}) - (f_2 - \sqrt{x^2 + y^2 + f_2^2})] \\ \varphi_2^{\mathrm{LCP}}(x, y) = -\dfrac{\pi}{\lambda}[(f_1 - \sqrt{x^2 + y^2 + f_1^2}) + (f_2 - \sqrt{x^2 + y^2 + f_2^2})] \\ \qquad\qquad + \dfrac{\pi}{\lambda}[(f_1 - \sqrt{x^2 + y^2 + f_1^2}) - (f_2 - \sqrt{x^2 + y^2 + f_2^2})] \end{cases}. \tag{2}$$

The first term on the right-hand side of equation (2) is referred to as the common part, and the second term as the different part of phase shift for $\varphi_1^{\mathrm{RCP}}(x, y)$ and $\varphi_1^{\mathrm{RCP}}(x, y)$. According to the property of propagation phase, the common part of the phase shift, i.e. $\frac{\varphi_1^{\mathrm{RCP}}(x,y) + \varphi_2^{\mathrm{LCP}}(x,y)}{2}$, can be tuned by propagation phase, i.e. $\varphi_{\mathrm{pro}}(x, y)$. Due to geometric phase imparting opposite and equal phase on the RCP and LCP incident lights, the different part of the phase shift, i.e. $\frac{\varphi_1^{\mathrm{RCP}}(x,y) - \varphi_2^{\mathrm{LCP}}(x,y)}{2}$, can be tuned by geometric phase, i.e. $\varphi_{\mathrm{geo}}(x, y)$. Hence, we have

$$\begin{cases} \varphi_{\mathrm{pro}}(x, y) = \dfrac{\varphi_1^{\mathrm{RCP}}(x, y) + \varphi_2^{\mathrm{LCP}}(x, y)}{2} \\ \varphi_{\mathrm{geo}}(x, y) = \dfrac{\varphi_1^{\mathrm{RCP}}(x, y) - \varphi_2^{\mathrm{LCP}}(x, y)}{2} \end{cases}. \tag{3}$$

It can be seen that only the geometric phase modulation works when $\varphi_1^{\mathrm{RCP}}(x, y) = -\varphi_2^{\mathrm{LCP}}(x, y)$. In contrast, the phase delay is only provided by propagation phase when $\varphi_1^{\mathrm{RCP}}(x, y) = \varphi_2^{\mathrm{LCP}}(x, y)$. Therefore, to make both type of

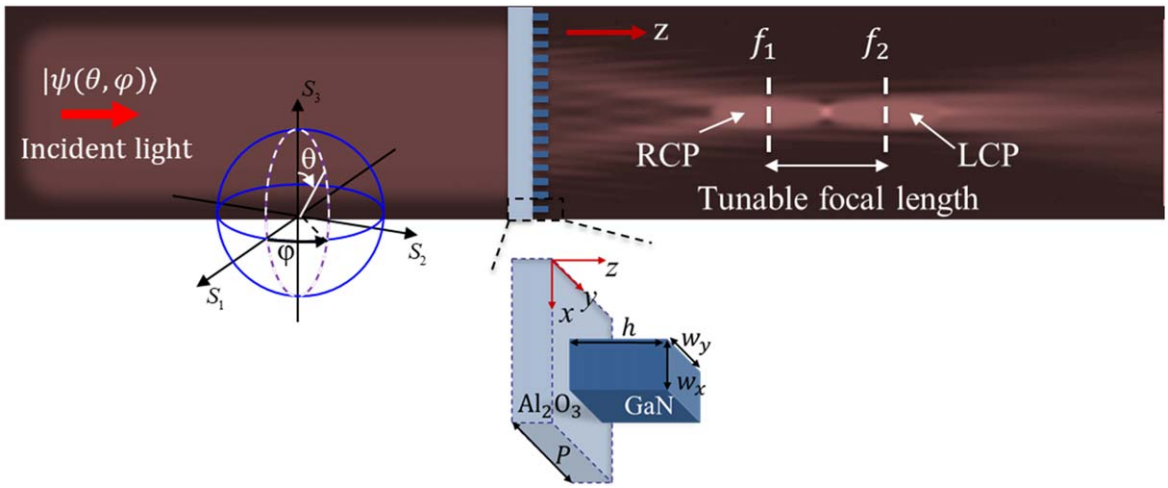

Figure 1. Schematic of the working principle of the proposed metalens with tunable focal length, where the incident light with arbitrary polarization state. The lower panel shows the unit cell of GaN nanopillar.

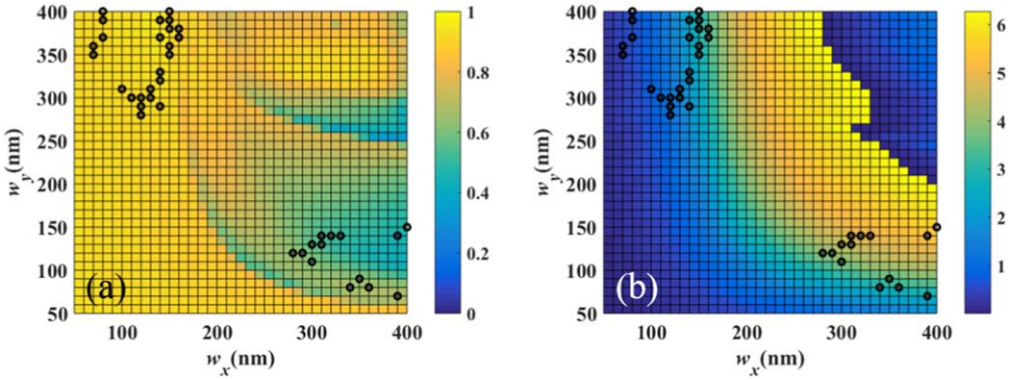

Figure 2. Dependence of transmittance T_x (a) and phase ψ_x on the structure parameters of the GaN nanopillar. Black dots represent the selected structures for the designed metalens. The wavelength is $\lambda = 633$ nm.

phases works simultaneously, it is straightforward to design a metalens with different focal lengths for RCP and LCP lights.

As the inset shows in figure 1, the polarization state of incident light with coordinate pair (θ, φ) on the Poincaré sphere can be decomposed into an RCP light and an LCP light as the following form

$$|\psi(\theta, \varphi)\rangle = \cos(\theta/2)e^{i\varphi/2}|R\rangle + \sin(\theta/2)e^{-i\varphi/2}|L\rangle. \quad (4)$$

By changing the polarization state of incident light, the ratio and the phase shift between the RCP light and LCP light can be tuned continuously. Consequently, when the designed focal lengths for RCP and LCP lights are reasonably far away from each other, it is feasible to tune the total focusing effect by varying the polarization state of the incident light.

3. Simulation and discussion

To verify the proposed method, we conduct a numerical experiment using the commercial software Lumerical FDTD solutions. In order to achieve a high light-focusing efficiency, the material should have negligible absorption with relatively high refractive index at visible wavelengths. Here, gallium nitride (GaN) is selected for the nanopillars and alumina material (Al_2O_3) as the substrate with permittivity extracted from [37]. Figure 1 shows the unit cell of the simulated GaN nanopillar. Periodic boundary conditions are applied along the x- and y-axes and perfectly matched layer (PML) boundary is applied along the z-axis. The x-polarized plane wave is normally incident on the sample to calculate the transmittance and phase delay. It should be noted that phase modulation instead of amplitude is used for the metalens, hence the transmittance of GaN nanopillars should be uniform. We set the period and height of the nanopillars to be 450 and 600 nm, respectively. Then, the width of the nanopillars along the x- and y-axes are scanned from 50 to 400 nm at intervals of 10 nm to obtain the transmittance and phase of the transmitted electric field. The transmittance T_x and phase response ψ_x of the transmitted electric field are shown in the figures 2(a) and (b), respectively. T_y and ψ_y can be obtained by interconverting of the x- and y-axes of figures 2(a) and (b). It can be seen that the phase change range covers $0 \sim 2\pi$, which satisfies the requirement of propagation phase modulation.

According to equation (1), once given the focal lengths for RCP and LCP incident lights, the phase modulation distributions of the metalens for the two orthogonal polarization states can be obtained. Next, the phase distributions, i.e. $\varphi_1^{\mathrm{RCP}}(x, y)$ and $\varphi_2^{\mathrm{LCP}}(x, y)$ can be decomposed into geometric phase $\varphi_{\mathrm{geo}}(x, y)$ and propagation phase $\varphi_{\mathrm{pro}}(x, y)$ components by equation (3). Furthermore, to achieve a high polarization conversion efficiency, we only need pillars whose phase response difference between the x and y directions is π according to the geometric phase modulation mechanism. Ideally, $T_x = T_y$ and $\psi_x = \psi_y \pm \pi$. Finally, the optimal structure of GaN nanopillar can be found by searching the scanned results in figures 2(a) and (b) by minimizing the modulation error $\Delta = \max[|T_{\mathrm{avg}} e^{i\varphi_{\mathrm{pro}}(x,y)} - T_x e^{i\psi_x}|, |T_{\mathrm{avg}} e^{i\varphi_{\mathrm{pro}}(x,y)\pm i\pi} - T_y e^{i\psi_y}|]$, which is similar to the method proposed in [31]. To manifest the tunable performance, the focal lengths of LCP and RCP incident light are set to be 90 and 100 μm, respectively. In our simulations, the total width of the proposed metalens is 50 μm, so there will be 111 nanopillars in one metalens. Periodic boundary condition is applied along y-axis and PML boundary is applied along the x- and z-axes. In order to improve the simulation efficiency, we only simulated a one-dimensional metalens. The GaN nanopillars used to form the metalens are selected as black dots shown in figures 2(a) and (b), whose quantitative transmittance and phase response is presented in table 1 in the supplementary materials (SMs), available online at stacks.iop.org/JOPT/21/115102/mmedia. The phase response difference between the x and y directions of each selected GaN nanopillars is almost equal to π. In addition, their transmittance of the selected GaN nanopillars has small fluctuations, of which the transmittance T_x is not exactly equal to T_y.

To evaluate the focusing performance, the transmitted field distribution of the metalens for RCP and LCP incident lights are calculated numerically. The polarization conversion efficiency of the metalens from LCP incident light to RCP transmitted light is 56.9% and co-polarized counterpart (from LCP incident light to LCP transmitted light) is 10.2%. Inversely, the polarization conversion efficiency from RCP to LCP is 54.9% and from RCP to RCP is 10.5% for RCP incident light. Then, according to equation (4), the field intensity distribution for arbitrary incident polarization state can be obtained by the coherent superposition of RCP and LCP incident light. Figure 3(a) shows the evolution of field intensity distributions for $\psi = 60°$ by varying the polarization state θ of the incident light. Distributions of the field intensity with ± 5 nm and ± 10 nm fabrication errors in the width of the nanopillars both along the x- and y-axes are presented in SMs, which shows the robustness of the proposed metalens. Figure 3(b) shows the quantitative relationship of the focal length between simulation results and the polarization state of the incident light (solid lines). For RCP and LCP incident lights, the focal length is consistent with the theoretical preset. A focal length varies from 88.9 to 98.6 μm can be realized. Since the focus tuning is realized by a superposition of RCP and LCP lights, the focus tuning range is limited by the focal

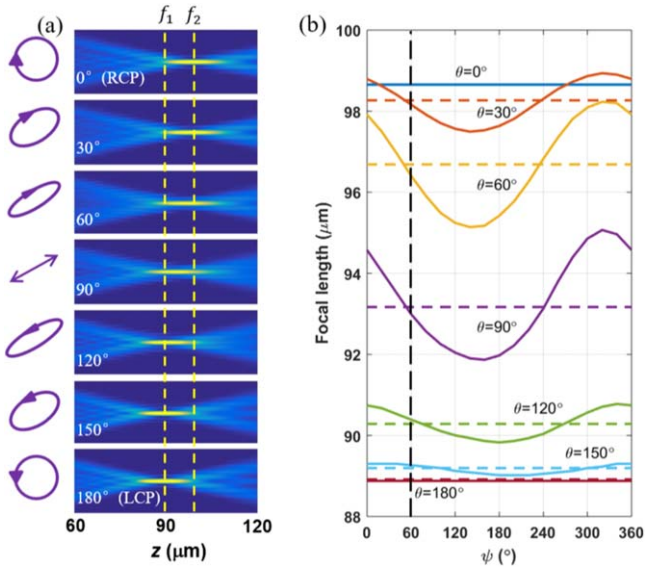

Figure 3. (a) Distributions of the field intensity of the polarization-enabled tuning focusing when $\psi = 60°$. Polarization state of the incident light is illustrated on the left column of (a). Two yellow lines represent the focal length of the designed metalens for RCP and LCP lights. (b) Evolution of the focal length by varing the polarization state of the incident light. Solid lines and dashed lines represent the focal length extracted from the total transmitted fields and only the cross-polarized fields, respectively. All the field and focal lengths are plotted at $\lambda = 633$ nm.

depth of the metalens for each CPLs. For this reason, the tuning range can be enlarged by decreasing the numerical aperture (NA) of the metalens. The focusing efficiency, defined as the ratio of intensity at the focal spot center to the incident intensity, is 63.1% for an LCP incident light and 59.9% for an RCP incident light at $\lambda = 633$ nm. Due to the existing of co-polarized light in the transmission space, the final field distribution of the focusing light is distorted slightly, which accounts for the fluctuation of the focal length, as the solid lines shown in figure 3(b). To stimulate the ideal metalens, we decompose the transmitted field of the metalens to extract the cross-polarized components for RCP and LCP incident lights, respectively. Furthermore, according to equation (4), the synthetic transmitted light field can be obtained for ideal metalens using the extracted cross-polarized components (dashed lines in figure 3(b)). Due to the orthogonality of RCP and LCP lights, the focal length of the ideal metalens varies with the azimuth angle θ of the incident light, but does not change with the declination angle φ of the incident light.

To characterize the focusing performance, the full-width at half-maxima (FWHM) of the focal spot along the x-axis (figure 4(a)) and focal depth along the z-axis (figure 4(b)) are normalized to their designer wavelength of 633 nm. As polarization state of the incident light rotates, the FWHM of the focal spot varies from 1.6 to 1.9 λ, which is close to the diffraction-limited FWHM $= 0.5\ \lambda/\mathrm{NA}$ [8], while the focal depth varies from 23.3 to 38.3 λ. It can be seen from figure 4(b) when θ approaches 0° or 180°, the focal depth decreases gradually, due to only the RCP or LCP incident

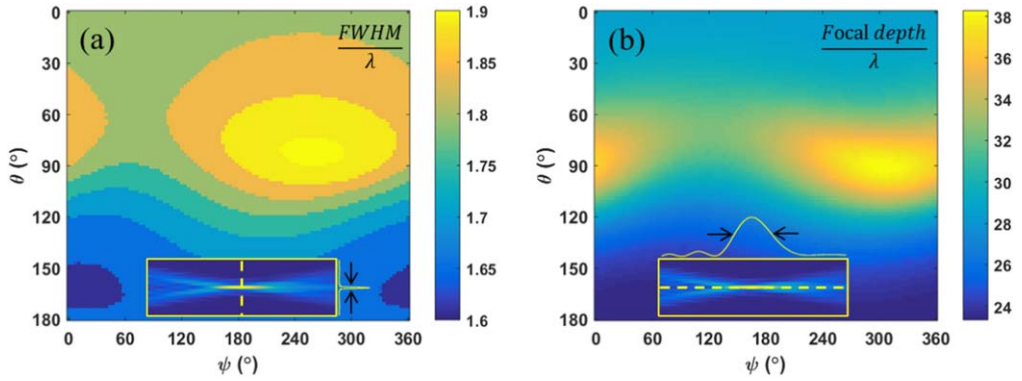

Figure 4. Dependence of the FWHM (a) and focal depth (b) of the focal spot on the polarization state of incident light.

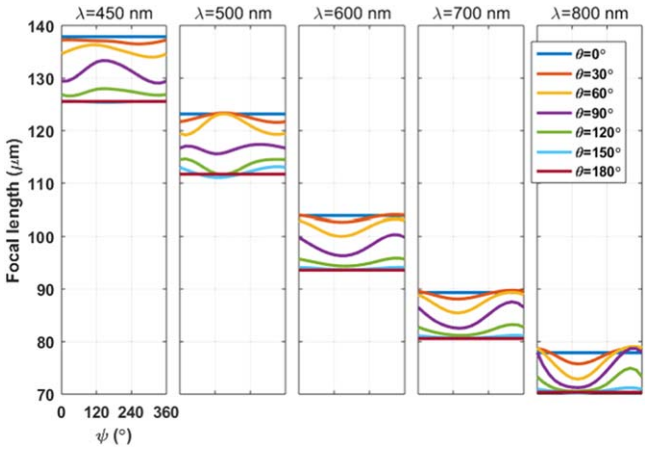

Figure 5. Broadband response of tunable focal length by varing the polarization state of incident light.

light contributing to the focusing performance. In contrast, the focal depth reaches at high level when θ approaches 90°. This is because both the RCP and LCP incident light contribute to the focusing performance.

Notably, the tunable focusing effect can almost be realized at the entire visible band, as shown in figure 5. The geometric phase component $\varphi_{geo}(x, y)$ is dispersion-free. However the propagation phase $\varphi_{pro}(x, y)$ is still affected by dispersion. Hence, it can be seen that the focal spot shift longitudinally as the wavelength and polarization state of incident light varies. The entire focal length varies from almost 70 to 138 μm when the wavelength of incident light changes from 800 to 450 nm. We also calculate the focusing efficiency of the metalens under RCP and LCP incident light at different wavelengths. The focusing efficiency is 13.2% at 450 nm, 32.7% at 500 nm, 61.8% at 600 nm, 55.0% at 700 nm, 37.3% at 800 nm for LCP incident light, and the focusing efficiency is 14.5% at 450 nm, 35.8% at 500 nm, 59.2% at 600 nm, 53.0% at 700 nm, 36.1% at 800 nm for RCP incident light. According the principle of geometric and propagation phases, the total focusing efficiency can be improved by selecting proper structures with low loss and efficient polarization conversion between CPLs. The corresponding NA of the metalens varies continuously from 0.178 to 0.336. The ratio of the adjustable focus range to the clear aperture of the metalens is close to 1.36, which is expected to be used for three-dimensional imaging for biological tissues or other transmissive objects.

4. Conclusion

In conclusion, we propose a metalens with polarization-enabled focal length tuning at almost the entire visible frequency by combining the geometric and propagation phases. By controlling the polarization state of incident light, the focal length of the metalens can be tuned dynamically. A focal length tuning range of 15 λ is realized at 633 nm. Compared to previous tunable metalenses, the proposed metalens maintains low structure complexity, which can find various applications in bioimaging and light beam modulation.

Acknowledgments

This work is supported by grants from the National Natural Science Foundation of China (Nos. 61805199, 11604256, 61875181 and 61705085), the Natural Science Foundation of Shaanxi Province, China (Nos. 2018JQ6065, 2018JM6001) and Special Zone for National Defense Science and Technology Innovation, China (No. 18-H863-01-ZT-001-004-02). The authors acknowledge CAS Pioneer Hundred Talents Program, 'the Fundamental Research Funds for the Central Universities' in China and the support from the University of Science and Technology of China's Centre for Micro and Nanoscale Research and Fabrication.

ORCID iDs

Lei Zhang https://orcid.org/0000-0002-5113-1786

References

[1] Yu N, Genevet P, Kats M A, Aieta F, Tetienne J P, Capasso F and Gaburro Z 2011 Light propagation with phase discontinuities: generalized laws of reflection and refraction *Science* **334** 333–7

[2] Zhang L, Mei S, Huang K and Qiu C-W 2016 Advances in full control of electromagnetic waves with metasurfaces *Adv. Opt. Mater.* **4** 818–33

[3] Yu N and Capasso F 2014 Flat optics with designer metasurfaces *Nat. Mater.* **13** 139–50

[4] Lee J Y, Kim Y, Han S, Kim J, Yoon J W, Lee K Y, Song S H, Yang K and Lee C S 2018 CMOS-compatible Si metasurface at visible wavelengths prepared by low-temperature green laser annealing *Nanotechnology* **30** 045301

[5] Chen X, Huang L, Mühlenbernd H, Li G, Bai B, Tan Q, Jin G, Qiu C-W, Zhang S and Zentgraf T 2012 Dual-polarity plasmonic metalens for visible light *Nat. Commun.* **3** 1198

[6] Wang W, Guo Z, Zhou K, Sun Y, Shen F, Li Y, Qu S and Liu S 2015 Polarization-independent longitudinal multi-focusing metalens *Opt. Express* **23** 29855–66

[7] Chen X, Chen M, Mehmood M Q, Wen D, Yue F, Qiu C-W and Zhang S 2015 Longitudinal multifoci metalens for circularly polarized light *Adv. Opt. Mater.* **3** 1201–6

[8] Khorasaninejad M, Chen W T, Devlin R C, Oh J, Zhu A Y and Capasso F 2016 Metalenses at visible wavelengths: diffraction-limited focusing and subwavelength resolution imaging *Science* **352** 1190–4

[9] Zhu A Y, Rousso D, Capasso F, Oh J, Khorasaninejad M, Devlin R and Chen W T 2016 Multispectral chiral imaging with a planar lens *Nano Lett.* **16** 4595–600

[10] Paniagua-Dominguez R, Yu Y, Khaidarov E, Choi S, Leong V, Bakker R M, Liang X, Fu Y H, Valuckas V and Krivitsky L A 2017 A metalens with near-unity numerical aperture *Nano Lett.* **18** 2124–32

[11] Chen W T, Zhu A Y, Sanjeev V, Khorasaninejad M, Shi Z, Lee E and Capasso F 2018 A broadband achromatic metalens for focusing and imaging in the visible *Nat. Nanotechnol.* **13** 220–6

[12] Faraji-Dana M, Arbabi E, Arbabi A, Kamali S M and Faraon A 2018 Compact folded metasurface spectrometer *Nat. Commun.* **9** 4196

[13] Lee G Y, Hong J Y, Hwang S, Moon S, Kang H, Jeon S, Kim H, Jeong J H and Lee B 2018 Metasurface eyepiece for augmented reality *Nat. Commun.* **9** 4562

[14] Huang K, Qin F, Liu H, Ye H, Qiu C-W, Hong M, Luk'yanchuk B and Teng J 2018 Planar diffractive lenses: fundamentals, functionalities, and applications *Adv. Mater.* **30** 1704556

[15] Hu X, Wen L, Song S and Chen Q 2015 Tunable graphene metasurfaces by discontinuous Pancharatnam–Berry phase shift *Nanotechnology* **26** 505203

[16] Liu J, Huang L, Zentgraf T, Li T and Wang Y 2017 Tunable wave plate based on active plasmonic metasurfaces *Opt. Express* **25** 4216

[17] Wan X, Qi M Q, Chen T Y and Cui T J 2016 Field-programmable beam reconfiguring based on digitally-controlled coding metasurface *Sci. Rep.* **6** 20663

[18] Dabidian N, Kholmanov I, Khanikaev A B, Tatar K, Trendafilov S, Mousavi S H, Magnuson C, Ruoff R S and Shvets G 2015 Electrical switching of infrared light using graphene integration with plasmonic fano resonant metasurfaces *ACS Photonics* **2** 216–27

[19] Donner J S, Morales-Dalmau J, Alda I, Marty R and Quidant R 2015 Fast and transparent adaptive lens based on plasmonic heating *ACS Photonics* **2** 355–60

[20] Jürgen S, Isabelle S, Manuel D, Evgenia R, Neshev D N, Igal B and Kivshar Y S 2015 Active tuning of all-dielectric metasurfaces *ACS Nano* **9** 4308–15

[21] Zhong J, Ning A, Yi N, Zhu M, Song Q and Xiao S 2016 Broadband and tunable-focus flat lens with dielectric metasurface *Plasmonics* **11** 537–41

[22] Chen K *et al* 2017 A reconfigurable active huygens' metalens *Adv. Mater.* **29** 1606422

[23] Ding P, Li Y, Shao L, Tian X, Wang J and Fan C 2018 Graphene aperture-based metalens for dynamic focusing of terahertz waves *Opt. Express* **26** 28038–50

[24] Ee H S and Agarwal R 2016 Tunable metasurface and flat optical zoom lens on a stretchable substrate *Nano Lett.* **16** 2818–23

[25] Kamali S M, Arbabi E, Arbabi A, Horie Y and Faraon A 2016 Highly tunable elastic dielectric metasurface lenses *Laser Photonics Rev.* **10** 1002–8

[26] Arbabi E, Arbabi A, Kamali S M, Horie Y, Faraji-Dana M and Faraon A 2018 MEMS-tunable dielectric metasurface lens *Nat. Commun.* **9** 812

[27] She A, Zhang S, Shian S, Clarke D R and Capasso F 2018 Adaptive metalenses with simultaneous electrical control of focal length, astigmatism, and shift *Sci. Adv.* **4** eaap9957

[28] Papaioannou M, Plum E, Rogers E T and Zheludev N I 2018 All-optical dynamic focusing of light via coherent absorption in a plasmonic metasurface *Light Sci. Appl.* **7** 17157

[29] Zhang L, Dong Z, Wang Y M, Liu Y J, Zhang S, Yang J K W and Qiu C-W 2015 Dynamically configurable hybridization of plasmon modes in nanoring dimer arrays *Nanoscale* **7** 12018–22

[30] Arbabi A, Horie Y, Bagheri M and Faraon A 2015 Dielectric metasurfaces for complete control of phase and polarization with subwavelength spatial resolution and high transmission *Nat. Nanotechnol.* **10** 937

[31] Balthasar Mueller J P, Rubin N A, Devlin R C, Groever B and Capasso F 2017 Metasurface polarization optics: independent phase control of arbitrary orthogonal states of polarization *Phys. Rev. Lett.* **118** 113901

[32] Devlin R C, Ambrosio A, Rubin N A, Balthasar Mueller J P and Capasso F 2017 Arbitrary spin-to-orbital angular momentum conversion of light *Science* **358** 896–901

[33] Li S, Li X, Wang G, Liu S, Zhang L, Zeng C, Wang L, Sun Q, Zhao W and Zhang W Multidimensional manipulation of photonic spin hall effect with a single-layer dielectric metasurface *Adv. Opt. Mater.* **7** 1801365

[34] Pancharatnam S 1956 Generalized theory of interference, and its applications *Proc. Indian Acad. Sci.* A **44** 247–62

[35] Berry M V 1987 The adiabatic phase and pancharatnam's phase for polarized light *J. Mod. Opt.* **34** 1401–7

[36] Huang L, Chen X, Mühlenbernd H, Li G, Bai B, Tan Q, Jin G, Zentgraf T and Zhang S 2012 Dispersionless phase discontinuities for controlling light propagation *Nano Lett.* **12** 5750–5

[37] Thomas M E and Tropf W J 1998 *Handbook of Optical Constants* ed P D Palik (San Diego, CA: Academic)